Comparative Investigation of Underpotential Deposition of Ag from Aqueous and Ionic Electrolytes: An Electrochemical and In Situ STM Study

D. Borissov, C. L. Aravinda, and W. Freyland*

University of Karlsruhe, Institute of Physical Chemistry, Kaiserstrasse 12, 76128 Karlsruhe, Germany

Received: December 14, 2004; In Final Form: April 11, 2005

Underpotential deposition (UPD) of Ag on Au(111) has been studied with two different electrolytes: aqueous 0.1 M H_2SO_4 solution in comparison with the ionic liquid 1-butyl-3-methylimidazolium chloride BMICl + $AlCl_3$. Of particular interest is the distinct behavior of 2D phase formation at both interfaces, which has been investigated by cyclic and linear sweep voltammetry in combination with in situ electrochemical scanning tunneling microscopy (STM). It is found that one monolayer (ML) of Ag is formed in the UPD region in both electrolytes. In aqueous solution, atomically resolved STM images at 500 mV versus Ag/Ag^+ show a (3 × 3) adlayer of Ag, whereas after sweeping the potential just before the commencement of the bulk Ag deposition, a transition from expanded (3 × 3) to pseudomorphic ML of Ag on Au(111) occurs. In BMICl−$AlCl_3$, the first UPD process of Ag exhibits two peaks at 410 and 230 mV indicating that two distinct processes on the surface take place. For the first time, STM images with atomic resolution reveal a transition from an inhomogeneous to an ordered phase with a $(\sqrt{3} \times \sqrt{3})R30°$ structure and an adsorption of $AlCl_4^-$ anions having a superlattice of $(1.65 \times \sqrt{3})R30°$ preceding the deposition of Ag.

I. Introduction

With the growing demand for nanostructured materials, the interest in fabrication and characterization of low-dimensional systems is continuously strong. In comparison with vapor deposition methods performed under ultrahigh vacuum (UHV) conditions, electrochemical deposition can be realized close to equilibrium. In combination with in situ scanning probe microscopy (SPM), the initial stages of electrochemical phase formation and growth can be resolved in real space on an atomic or nanometer scale.[1−3] By limiting the deposition potential to values positive of the bulk Nernst potential (underpotential deposition, UPD), the formation and dissolution of low-dimensional structures can be studied.[4] UPD of metals has been studied extensively both by conventional electrochemical methods and by different spectroscopic and structural techniques including SPM. In particular, phenomena of 2D phase formation and transitions as well as anion adsorption/desorption have been investigated in detail for several 2D metal systems; see, for example, refs 5 and 6.

In most of these investigations, aqueous electrolytes have been employed. Recently, it has been shown that electrochemical SPM experiments are feasible at ionic liquid/solid interfaces with resolution comparable to that achieved in aqueous solutions.[7,8] The special advantage of these electrolytes are their relatively wide electrochemical windows which enable the electrodeposition of a larger number of metals and, in particular, of semiconductors.[9,10] In addition, the effect of hydrogen evolution and its influence on the morphology of the deposit can be avoided in ionic liquid electrolytes.

In this contribution, we focus on the UPD of Ag on Au(111) in ionic liquid, $AlCl_3$−BMICl, in comparison to the UPD process in aqueous H_2SO_4 solution. We particularly address the problem of anion adsorption/desorption at the respective interfaces and the differences/similarities in the Ag adlayer formation. This is studied by cyclic voltammetry, linear sweep voltammetry, and electrochemical scanning tunneling microscopy.

II. Experimental Section

The underpotential deposition of silver was examined on an Au(111) single-crystal electrode (10 mm × 10 mm, MaTeck, Germany). For electrochemical and in situ STM experiments, the single crystal was electrochemically polished in a solution of 0.5 M H_2SO_4 at constant voltage of 4 V (vs Pt counter electrode) for 60 s, and the resulting oxide layer was dissolved in 1 M HCl for a couple of minutes. Prior to use, the substrate was annealed in a hydrogen flame for 10 min and then slowly cooled in a stream of nitrogen (Griesheim, 5 N). The silver plating solutions contained 1 mM Ag_2SO_4 (Merck, p.a.) with a supporting electrolyte of 0.1 M H_2SO_4 (Merck, Suprapur) prepared in Milli-Q water (Millipore, 18.2 MΩ) and 2 mM AgCl (Fluka, p.a.) in 58:42 mole ratio $AlCl_3$−1-butyl-3-methylimidazolium chloride (BMICl), respectively. The preparation and purification of the former are described elsewhere.[7] The electrochemical measurements were performed in a conventional three-electrode electrochemical cell. Silver and platinum wires were used as reference and counter electrodes. All potentials in this paper are quoted relative to the Ag/Ag^+ couple in both electrolytes. Cyclic voltammograms (CVs) were carried out with an AutoLab potentiostat (PGSTAT 30, Eco Chemie, The Netherlands). The aqueous electrolyte was purged with nitrogen before each experiment.

In situ scanning tunneling microscopy (STM) images were acquired in constant current mode using a Molecular Imaging PicoScan controller. Tungsten and Pt−Ir tunneling probes were employed. The tips were fabricated by etching in 2 M NaOH and in 3.5 M NaCN, respectively, followed by coating with electrophoretic paint (BASF ZQ 84-3225 0201) in order to minimize Faradaic currents. STM experiments were performed

* E-mail: werner.freyland@chemie.uni-karlsruhe.de (fax: ++49 721 608 6662).

10.1021/jp0443106 CCC: $30.25
Published on Web 05/19/2005

in an air-sealed chamber which was filled with argon and equipped with a home-built 2μ STM scanner. The scanner was calibrated against the lattice spacing of a highly ordered pyrolitic graphite (HOPG) surface for in-plane dimensions and against monatomic Au(111) steps for dimensions normal to the surface.[11] The STM images are not subjected to any numerical manipulation or image processing.

III. Results and Discussion

UPD of Ag on Au(111) in Aqueous 0.1 M H_2SO_4. A cyclic voltammogram recorded on a Au(111) single crystal in 1 mM Ag_2SO_4 + 0.1 M H_2SO_4 at a sweep rate of 30 mVs^{-1} is shown in Figure 1A. The UPD of Ag on Au(111) is characterized by two major pairs of voltammetric peaks at 520 mV (C1) and 25 mV (C3) indicating that two distinct processes occur on the surface in the underpotential region. A weak reversible redox couple is also apparent at 130 mV (C2). The voltammetry and the corresponding peak positions are in good agreement with literature.[12,13] At 520 mV (C1), the first UPD of Ag on Au(111) occurs with a corresponding anodic peak at 528 mV (A1). It is interesting to know how much charge is associated with the first peak. Therefore, sets of charge measurements were carried out by means of linear sweep voltammetry (LSV) employing the loop method with an initial potential of 600 mV, various final potentials, and polarization times of 300 s.[3] From this, a desorption isotherm has been derived, as shown in Figure 1B. It does not show a discontinuous drop of Q versus E near 520 mV as expected for a first-order phase transition below the critical temperature. This may have different origins. First, we cannot exclude a coadsorption of sulfate (bisulfate). Furthermore, the continuous drop of Q versus E can be due to a low critical temperature determined by weak adsorbate−adsorbate interactions. The charge consumed for the first UPD of Ag including the uncertainty of the double-layer charging correction was found to be 55 ± 10 μC cm^{-2}. By taking into account that 1 pseudomorphic monolayer (ML) of Ag is associated with a charge density of 222 μC cm^{-2}, the estimated silver coverage is 0.25 ML, suggesting the formation of a more open adlayer of silver. The value is smaller than those published in previous works.[12−15] There are, however, some inconsistencies in the reported coverage of the first UPD of Ag in sulfuric acid solutions. For instance, Itaya[12] and Mrozek[14] have derived the coverage from coulometry in the range 0.31−0.34 ML. In contrast, Gewirth[15] and Kolb[13] have employed charge measurements in order to estimate silver adatom coverage on Au(111) and have shown that the surface coverage of Ag in the first UPD is about 0.45 ML. These discrepancies can be due to a specific coadsorption of sulfate on Au(111) which has been evidenced in the same potential range in which the first UPD of Ag occurs.[16,17] However, if surface alloying with a slow kinetics plays a significant role in the first UPD process, the charges derived in this study could be lower than those in the literature for the polarization times used. This can explain the inconsistency with the expected coverage for a (3 × 3) Ag structure too (see below).

The stripping current curves of Ag taken at a sweep rate of 10 mVs^{-1} after the substrate has been polarized at a certain potential in the range of the cathodic wave (C1) until the cathodic current is almost zero are presented in the inset of Figure 1B. In fact, the anodic stripping waves are divided into two peaks which occur at 528 and 539 mV. The double peak is already manifested in a shoulder of the peak (A1) in the voltammogram (Figure 1A). This feature has been observed and reproduced by independent measurements of different groups[12,13,15]

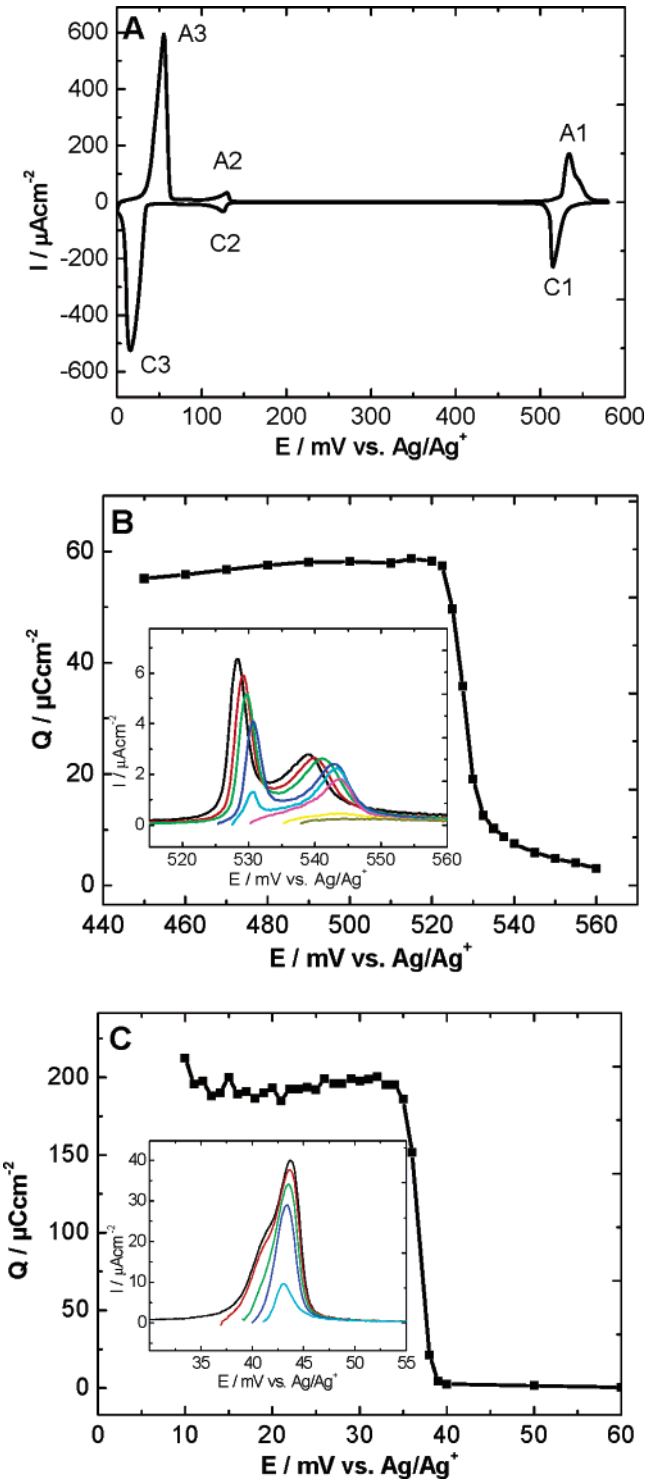

Figure 1. (A) Cyclic voltammogram recorded on single-crystal Au(111) in 1 mM Ag_2SO_4 + 0.1 M H_2SO_4 at a sweep rate of 30 mV s^{-1}. (B) Desorption isotherm for the first UPD of Ag at 520 mV derived from measurements using the loop technique. Inset shows the anodic linear sweep voltammograms with a sweep rate of 1 mV s^{-1} (see text). (C) Corresponding desorption isotherm for the second UPD of Ag at 40 mV s^{-1}. Inset shows the dissolution curves taken at 2 mV s^{-1}.

but has not been discussed further. Although a corresponding split in C1 is not seen in our voltammogram, it is apparent in these previous studies. In a separate set of LSV measurements not presented here, the potential difference between the two maxima (Figure 1B) was found to be 11 mV and appears to be independent of the sweep rate. These findings suggest that the silver adatoms occupy two different energetically favored sites

on the single-crystal Au(111), resulting in a double oxidative desorption peak which occurs at two distinct potentials indicating surface alloying. Further evidence supporting this conclusion will be given with the corresponding STM images. In addition, the adsorptive/desorptive properties of the substrate can depend on the crystal face. Thus, we should not exclude the fact that the difference in the shape, the size, and the number of the adsorptive/desorptive peaks in the CV can originate from adsorption/desorption of Ag adatoms on crystal faces other than (111) due to defects in the single crystal.

In respect to the second major redox peak at 25 mV (C3), the derived desorption isotherm shows that the charge density involved is 190 ± 36 μC cm^{-2} (Figure 1C). The charge density includes the contribution of the weak redox couple at 130 mV (C2) which is thought to be caused by a commensurate−incommensurate transition.[18] A brief assessment suggests that for both UPD processes of Ag the total charge density of 245 μC cm^{-2} can be ascribed to the formation of 1 Ag ML. This result is in agreement with the charge values published by Itaya.[12] On the other hand, Kolb et al. have reported much higher values in the range of 380 μC cm^{-2} assuming the formation of 2 ML.[13]

To conclude the CV results, the UPD of Ag exhibits two distinct surface processes. At 520 mV, an expanded adlayer of silver is formed corresponding to surface coverage of 0.25 ML. By sweeping the potential just before the commencement of the bulk Ag deposition, a transition from an expanded to a pseudomorphic monolayer of Ag on Au(111) seems to occur.

It is interesting to analyze how well the electrochemical examination of the UPD of Ag on Au(111) presented so far corresponds to in situ STM studies. In these experiments, attention was focused on the surface processes accompanying the first UPD of Ag (C1/A1). Figure 2A shows an in situ STM image of Ag on a large scan (500 nm × 500 nm) obtained at 500 mV. The STM image reveals a compact adlayer of Ag exhibiting a small number of monatomically deep holes and islands. The adlayer covers the whole surface following the topography of the substrate and terminates at the monatomic step edge of Au(111) as shown in Figure 2A. Moreover, a high-resolution image at the same potential reveals individual silver adatoms packed into an ordered adlayer exhibiting a spacing of 8.3 ± 0.5 Å and 8.7 ± 0.2 Å between the adjacent adatoms that have the same contrast (see Figure 2B). The interatomic distances suggest a (3 × 3) superlattice. A schematic representation of the adlayer with the (3 × 3) structure on Au(111) is given in Figure 1C in which the open circles represent Au(111) surface atoms, whereas the filled gray ones are Ag adatoms at atop sites, and filled black ones are Ag adatoms at bridging sites. The model clearly shows that silver atoms take both atop and twofold bridge sites. Interestingly, the pattern of alternating higher and lower rows is exactly what is seen in the STM image (Figure 1B). The modulation of height in the [11$\bar{0}$] direction is less pronounced than that in the [11$\bar{2}$] direction.

In comparison with previous studies, our findings are in good agreement with those of Gewirth et al.[15] who have found by AFM a (3 × 3) structure at 420 mV. The same structure has been deduced from low-energy electron diffraction (LEED) measurements by Mrozek et al., but in fluoride ion media.[14] In contrast, a ($\sqrt{3} \times \sqrt{3}$)*R*30° packing has been inferred by Itaya[12] in a broad potential region 500−200 mV. Similarly, Kolb has claimed that the ($\sqrt{3} \times \sqrt{3}$)*R*30° structure coexists with the (3 × 3) one at 500 mV.[13]

The (3 × 3) superlattice corresponds to a packing density of 0.44 ML, which is substantially higher than the charge-derived

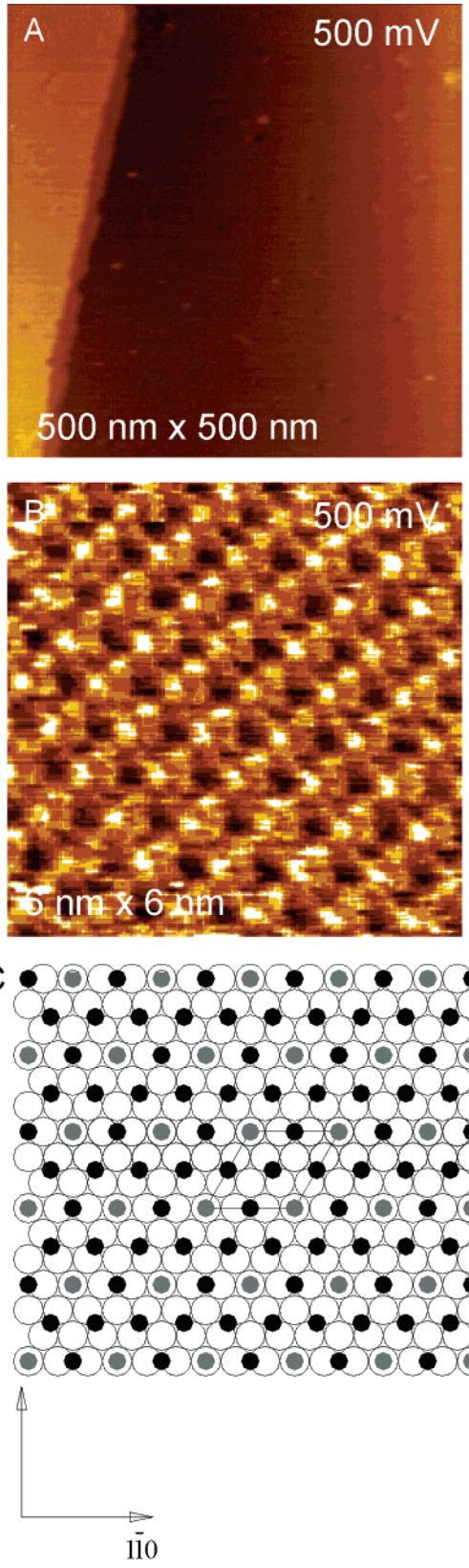

Figure 2. In situ STM images of the first UPD adlayer of Ag at 500 mV on Au(111), (A) Ag adlayer on a large scan of 500 nm × 500 nm. I_t = 0.5 nA, U_{bias} = −0.3 V. (B) Atomically resolved STM image of a 6 nm × 6 nm region of the Ag adlayer exhibiting interatomic spacing of 8.3 ± 0.5 Å and 8.7 ± 0.2 Å. The modulation of height in [11$\bar{2}$] is a result of alternating adatoms in atop and twofold bridging sites. I_t = 1 nA, U_{bias} = −0.2 V. (C) Schematic representation of (3 × 3) structure of Ag on Au(111). Note that small, filled gray circles represent Ag adatoms at atop sites, whereas the black ones represent Ag adatoms at bridging sites.

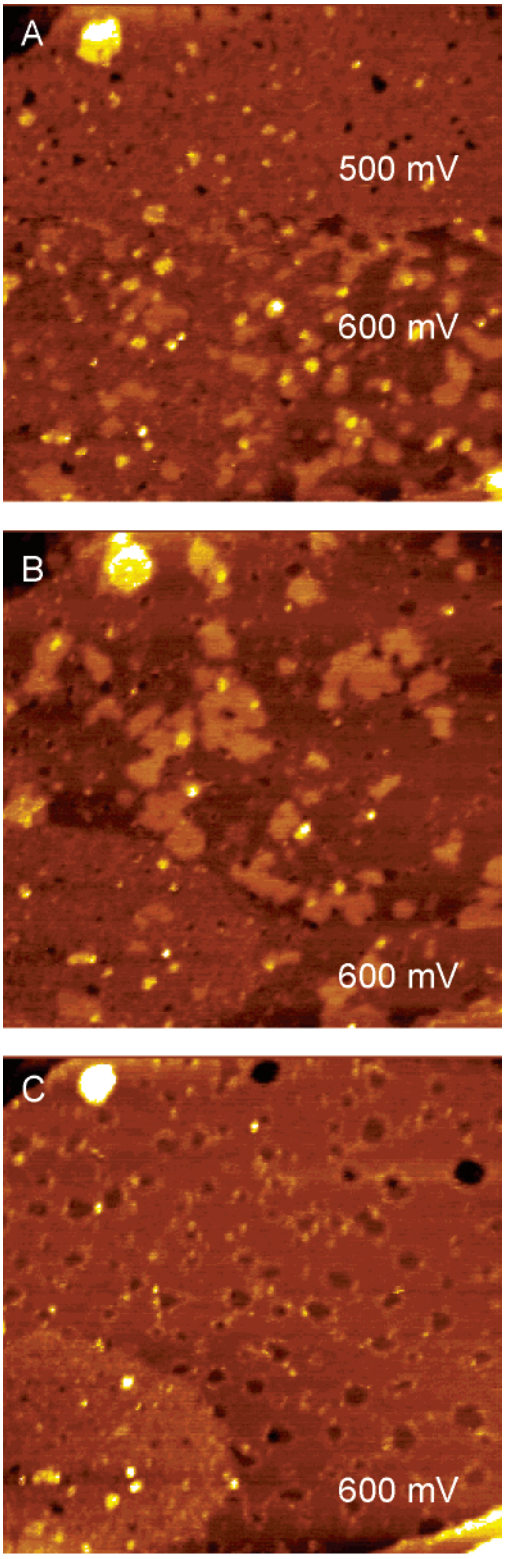

Figure 3. In situ STM images of stripping of the first UPD Ag adlayer on Au(111) in 1 mM Ag_2SO_4 + 0.1 M H_2SO_4 on a large scan of 175 nm × 175 nm. I_t = 1 nA, U_{bias} = −0.1 V. (A) In the middle of the scan, the potential was switched from 500 to 600 mV. The scanning direction is from top to bottom. (B) The next sequential scan at 600 mV shows that some islands of the adlayer of Ag still remain. (C) Two minutes later, the STM image reveals a number of pits in the Au(111) surface which are filled with Ag; the following scans show that Ag is utterly dissolved from the pits, resulting in the formation of monatomically deep gold pits.

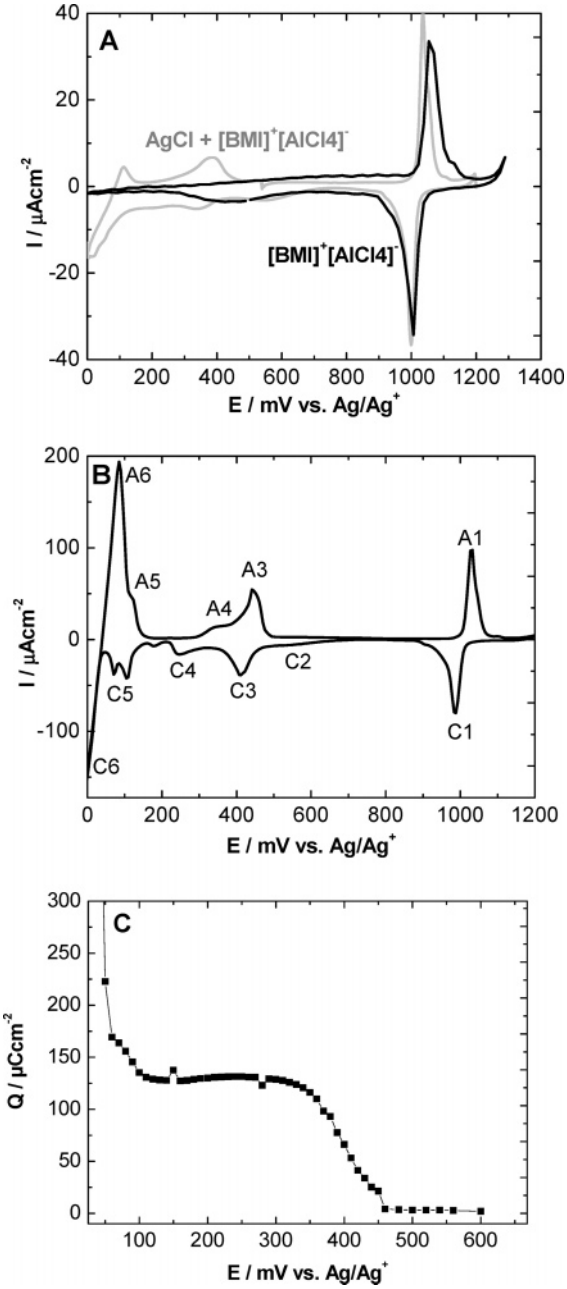

Figure 4. (A) Cyclic voltammogram recorded on single-crystal Au(111) at a sweep rate of 20 mV s^{-1} in 58:42 mole ratio $AlCl_3$−BMICl before (black line) and after (grey line) small amount of AgCl is added. (B) CV taken in 2 mM AgCl + $AlCl_3$/BMICl at a sweep rate of 50 mV s^{-1}. (C) Desorption isotherm derived from coulorimetric measurements in the whole UPD range of Ag.

coverage of this work. Although we have not observed anion coadsorption in the STM images, such a discrepancy could originate from coadsorption of sulfate anions overlapping with the first UPD of Ag and/or surface-alloyed Ag, which cannot be completely dissolved during the anodic sweep with 1 mV s^{-1} and is therefore underestimated in the charge-derived coverage.

The dissolution process of Ag for the first UPD on Au(111) is manifested by the sequential STM images presented in Figure 3. The potential was swept from 500 to 600 mV in the middle of the scan to elucidate the stripping of the (3 × 3) adlayer of Ag (Figure 3A). Some residuals of the layer are still observed in a short time at 600 mV (Figure 3B). After removal of Ag, a number of monatomically deep pits with diameters between 2

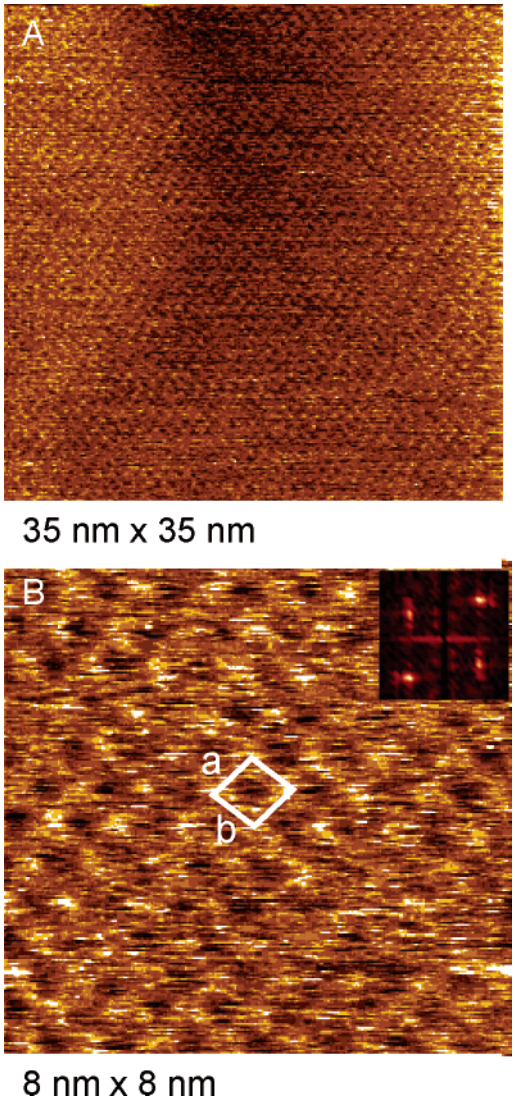

Figure 5. In-situ STM images of an ordered adlayer of $AlCl_4^-$ on Au(111) at 500 mV in $AlCl_3$−BMICl. $I_t = 1$ nA, $U_{bias} = 0.1$ V. (A) 35 nm × 35 nm region. (B) 8 nm × 8 nm region. Inset shows the superlattice of $AlCl_4^-$ derived from 2D FFT of the STM image yielding lattice constants of $a = 8.3 \pm 0.5$ Å and $b = 9.8 \pm 0.5$ Å.

and 10 nm are seen in the basal plane of the Au(111) (Figure 3C). These pits were found to anneal very slowly with time. Moreover, it is thought that an initial stage of oxidation of the gold preferentially takes place at the step sites as revealed from the corrugation of the step edges. It should be noted that similar pitting of the Au(111) terraces in sulfate[20] and perchlorate[21] solutions has been observed only by a potential excursion to 900 mV (1300 mV vs saturated calomel electrode, SCE)[19] and a subsequent reduction of the gold oxide species. Although special care was taken in our measurement that the substrate was not exposed to such high potentials, the formation of pits indicates that this is a consequence of the stripped layer of silver and its strong interaction with the underlying gold surface, which is indicative of surface alloying.

UPD of Ag on Au(111) in BMICl−$AlCl_3$. In a previous study of Ag electrodeposition on Au(111) in an acidic BMICl−$AlCl_3$ melt, it has been shown that the UPD process of Ag can be examined by in situ STM.[7] However, concerning the details of the nucleation and growth mechanism and, in particular, the atomic structure of the Ag adlayer, a number of questions remained open and are addressed in the current study. First of all, it is necessary to compare the voltammogram of the pure ionic electrolyte with the one obtained from a solution in which a 10-mg crystal of AgCl was dissolved in $[BMI]^+[AlCl_4]^-$. The comparison (Figure 4A) clearly shows that the silver-containing

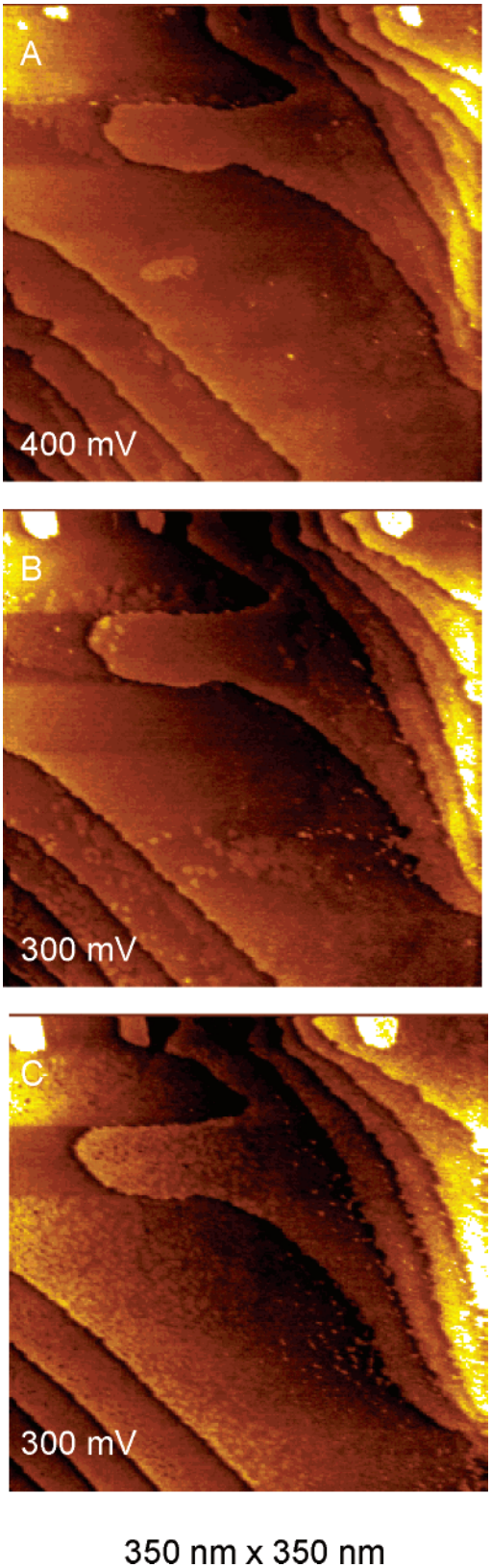

Figure 6. A sequence of in situ STM images (350 nm × 350 nm) showing the initial stages of nucleation and growth for the first UPD of Ag in $AlCl_3$−BMICl. $I_t = 1$ nA, $U_{bias} = 0.1$ V. At (A) 400 mV, (B) 300 mV, (C) Same as (B), but 8 min later.

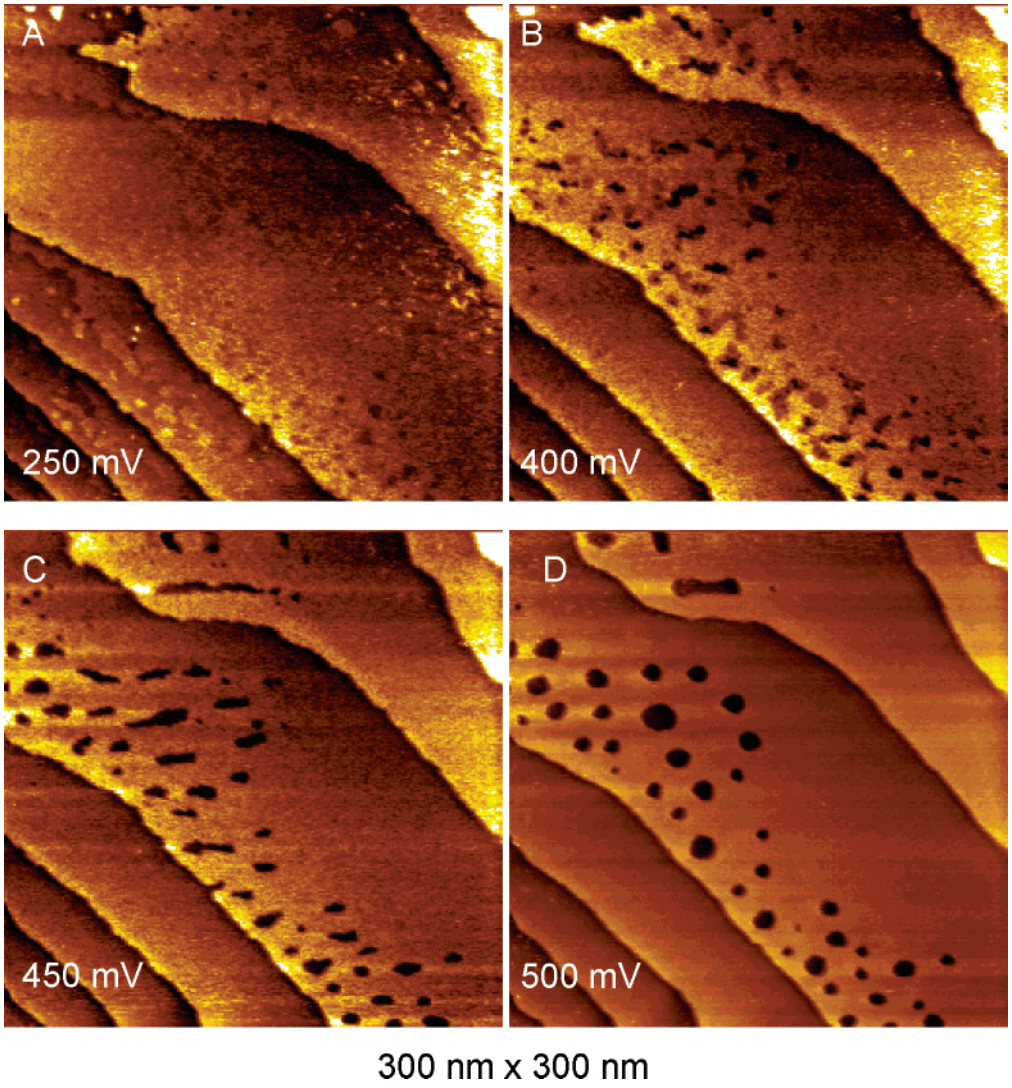

Figure 7. In situ STM images of the dissolution (300 nm × 300 nm) of the first Ag adlayer on Au(111) in $AlCl_3$−BMICl. $I_t = 1$ nA, $U_{bias} = 0.05$ V. At (A) 25, (B) 400, (C) 450, (D) 500 mV.

melt exhibits two additional redox couples around 350 and 50 mV, which we associate to the first and second UPD processes of Ag, respectively. A typical cyclic voltammogram recorded in 2 mM AgCl + $[BMI]^+[AlCl_4]^-$ on Au(111) at a sweep rate of 50 mV s^{-1} is shown in Figure 4B. The occurrence of the redox couple at 990 mV (C1) and 1025 mV (A1) was found to be independent of the content of silver in the melt, implying that the process is characteristic of the Au(111)−BMICl−$AlCl_3$ interface. A charge density of 73 ± 14 μC cm^{-2} was derived from the CV. This process has been ascribed to a 2D dissolution/deposition of gold occurring preferentially at step edges.[7] It is likely that during dissolution $AuCl_4^-$ species are formed and then chemisorbed on the surface. Further reducing the potential leads to their reduction and deposition. 3D dissolution of gold should be expected at more positive potentials, but the electrochemical window of the ionic liquid is limited to 1200 mV where decomposition of the ionic liquid arises.

Another interesting feature of the CV concerns the broadening in the range between 500 and 600 mV (C2), which is also independent of the content of Ag (see Figure 4A). In analogy with aqueous solutions, prior to the first UPD of Ag, we interpret this process as chemisorption of tetrachloroaluminate anions. Further evidence in this regard will be given by the STM images. According to the CV, the first UPD of silver arises at two different potentials at 410 mV (C3) and 230 mV (C4), indicating two distinct surface processes. The same is true for the second UPD at 120 and 106 mV. Surprisingly, continuous multilayer deposition of Ag starts at 40 mV (see also Figure 10). To clarify to what extent Ag covers the Au(111) surface in the respective UPD regions, a desorption isotherm was derived on the basis of coulometry. The isotherm presented in Figure 4C shows charge densities of 131 ± 25 μC cm^{-2} (0.59 ML) and 220 ± 42 μC cm^{-2} (0.99 ML) for the first and second UPD, respectively. This result clearly shows the formation of 1 ML in the UPD range as in aqueous solutions.

Prior to the first UPD process of Ag, the Au(111) surface was examined by STM at 550 mV. High-resolution imaging acquired at this potential reveals for the first time a well-ordered layer of chemisorbed tetrachloroaluminate anions on Au(111) (Figure 5). The first indication was reported by Stafford et al. who shown by means of STM an adsorption of tetrachloroaluminate species in acidic aluminum chloride/1-methyl-3-ethylimidazolium chloride on Cu(111).[22] The superlattice derived from the 2D fast Fourier transforms (FFT) of the STM data is presented in the inset of Figure 5B. The adsorbed tetrahedral ionic complex leads to a structure with lattice constants of a = 8.3 ± 0.5 Å and b = 9.8 ± 0.5 Å. The unit cell is equivalent to a $(1.65 \times \sqrt{3})R30°$ structure and seems to be incommensurate with the underlying Au(111). This conclusion is also supported by observing a Moiré pattern not presented here. It is thought

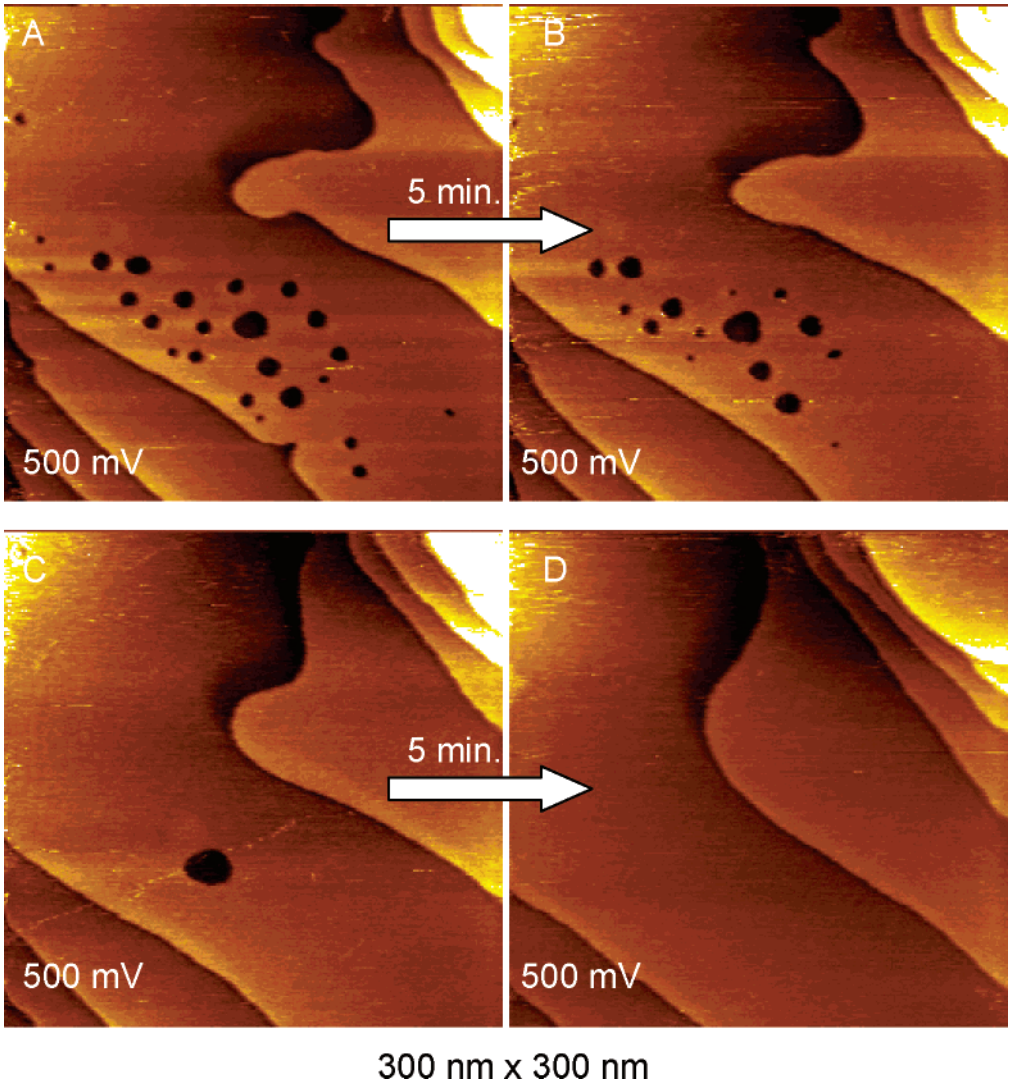

Figure 8. Sequence of in situ STM images (300 nm × 300 nm) at a constant potential of 500 mV after dissolution of the first Ag adlayer on Au(111) in $AlCl_3$−BMICl which shows the annealing of the pits in the surface with time. $I_t = 1$ nA, $U_{bias} = 0.05$ V. (A) 0, (B) 5, (C) 10, (D) 15 min.

that tetrachloroaluminate species are chemisorbed with the tetrahedral face adjacent to the Au(111).

By reducing the potential toward 400 mV, the first UPD of Ag takes place. The initial stage of the nucleation and growth process is manifested by the sequence of in situ STM images as shown in Figure 6. At 400 mV, a layer of Ag starts growing from the monatomic step edges as well as on the terraces of Au(111) (Figure 6A). The new silver phase seems to be less in height than a monatomic Au(111) step. Its growth at constant potential is demonstrated on a large-scan range of 350 nm × 350 nm (Figure 6B,C) within a time span of 8 min. At 300 mV, the 2D silver islands grow and merge with one another until a certain level. As a result, an inhomogeneous adlayer is formed with partial coverage. The same conclusion can be drawn on the basis of coulometry, from which 0.59 ML coverage is expected. This is in contrast to aqueous solutions where a homogeneous open (3 × 3) adlayer of silver develops after the first UPD (see Figure 2B).

Figure 7A−D illustrates the dissolution of the inhomogeneous adlayer when the potential is gradually stepped back to 500 mV. As in aqueous solutions, the dissolution of the Ag adlayer leads to a pitting in the Au(111) surface, but now with a very pronounced structure. After dissolution, numerous monatomically deep holes with diameters between 5 and 20 nm are seen all over the Au terraces as shown in Figure 7D. This observation is consistent with the previous STM study.[7] Because of the long polarization time, which was needed for acquisition of the STM images before the dissolution (about 30 min), we explain the pitting as a result of 2D Ag−Au surface alloying. This is supported by the observation of wormlike inhomogeneities (Figure 6C) and the corresponding wormlike defect structures (Figure 7B) which are indicative of a spinodal decomposition reaction governing surface alloying.[25]

Another set of subsequent STM images obtained at 500 mV after dissolution reveals that the monatomically deep pits disappear relatively rapidly with time; see Figure 8A−D. At first, the smaller pits vanish, and changes in the shape of the step edges become apparent as depicted in Figure 8C,D. The surface recovers very rapidly, within approximately 20 min, because of rapid surface diffusion of Au adatoms left on the surface after the dissolution of the Au_xAg_y surface alloy.[24] It is known that the rate of diffusion in the solution containing chloride ions is faster than that in a 0.1 M H_2SO_4 medium.[21,23] Therefore, such a difference in the kinetics of annealing the pits can be expected when comparing sulfuric solutions with ionic liquids.

Another interesting result concerns the fact that the first UPD of Ag on Au(111) in BMICl−$AlCl_3$ undergoes a completely

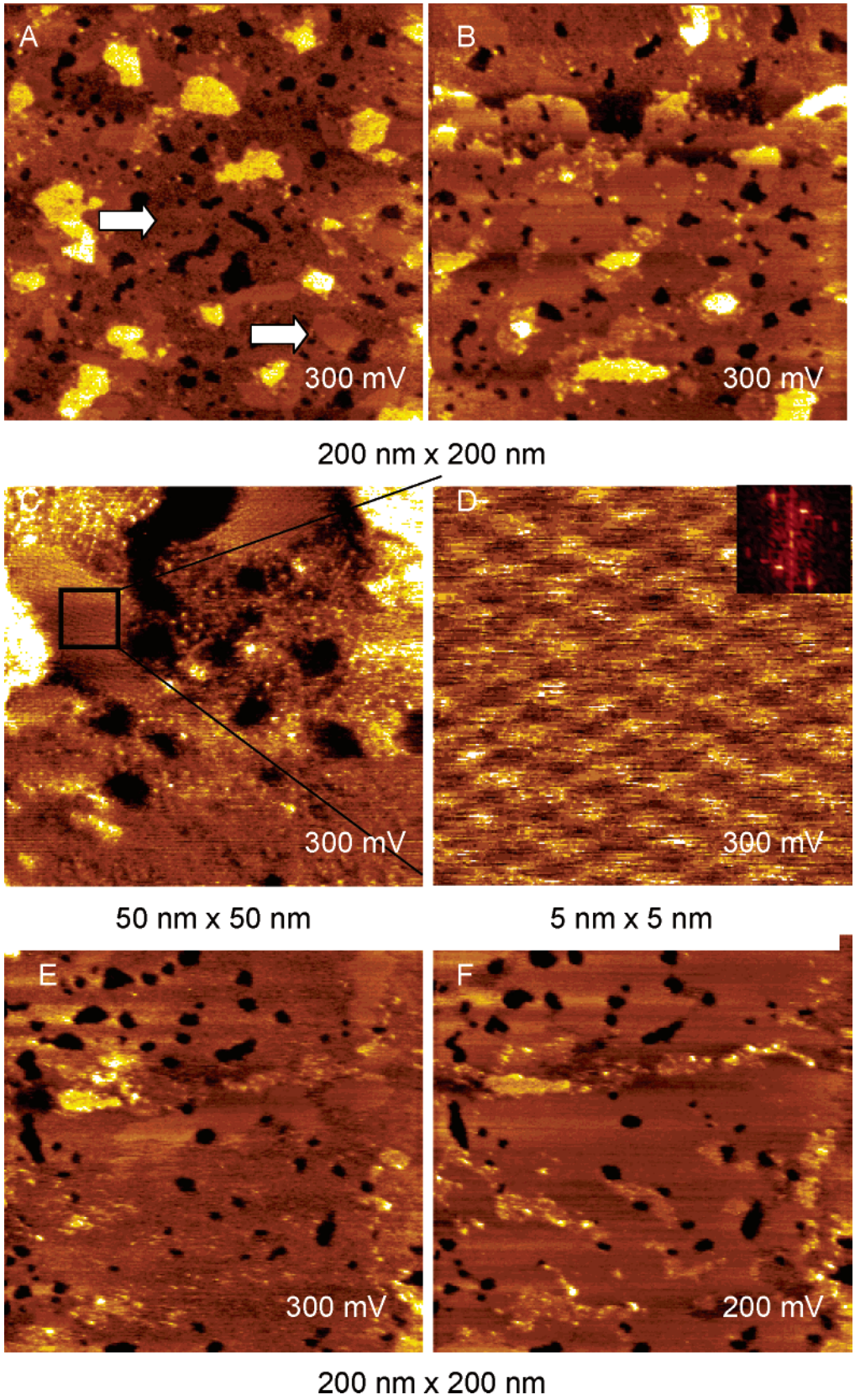

Figure 9. (A, B) In situ STM images (200 nm × 200 nm) of the first Ag adlayer on Au(111) in $AlCl_3$−BMICl at 300 mV. Arrows show domains of densely packed and disordered Ag phases. (C) 50 nm × 50 nm and (D) 5 nm × 5 nm high-resolution STM images of the densely packed Ag phase. Inset shows the superlattice of the packed Ag phase obtained from 2D FFT of the STM image yielding superlattice constants of 4.4 ± 0.6 Å and 5.6 ± 0.5 Å. STM images indicate disorder−order transitions when the potential is switched from (E) 300 mV to (F) 200 mV. The domains of the densely packed Ag adlayer expand at the expense of the disordered phase. $I_t = 1$ nA, $U_{bias} = 0.1$ V.

different mechanism in comparison with that in sulfuric media. As one can see from the CV (see Figure 4B), the first UPD of Ag has two distinct peaks separated by nearly 200 mV, whereas in aqueous solution, only one peak is observed. So, the question

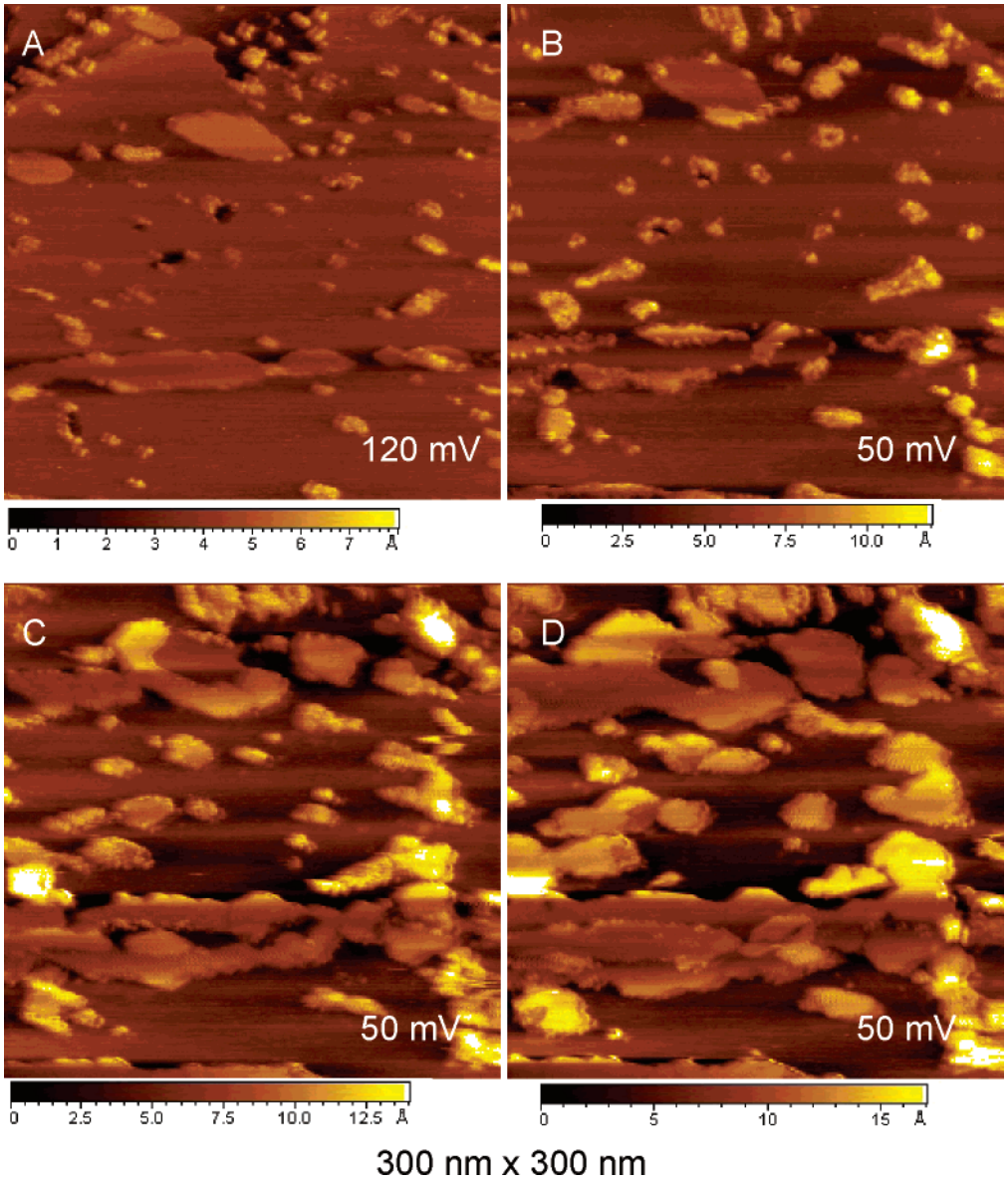

Figure 10. In situ STM images (300 nm × 300 nm) on Au(111) in $AlCl_3$−BMICl at (A) 120 and (B) 50 mV. (C) Next scan after 2 min; (D) 2 min later. $I_t = 1$ nA, $U_{bias} = 0.1$ V.

arises: What is the origin of these two peaks? To obtain an unambiguous answer, we have examined by STM the Ag adlayer on the Au(111) at a potential of 300 mV at which both processes related to the C3 and C4 peaks take place. On a large scan size of 200 nm × 200 nm (Figure 9A,B), the silver adlayer exhibits many inhomogeneities as well as monatomically deep holes. Moreover, we have found for the first time that two distinct domains of condensed and expanded surface structures of Ag coexist at 300 mV. The condensed structure (indicated with a pointer in Figure 9A) appears to be smoothed, whereas the expanded structure seems to be rough and atomically disordered (Figure 9C). An atomically resolved STM image of the condensed phase is depicted in Figure 9D. In this instance, the image reveals a well-ordered structure of the silver monolayer. 2D FFT of the STM data yields a typical unit cell (presented in the inset of Figure 9D) with interatomic distances of 4.4 ± 0.6 Å and 5.6 ± 0.5 Å. This result indicates that the silver adlayer in the condensed domains has a packing comparable to that of a compressed $(\sqrt{3} \times \sqrt{3})R30°$ monolayer. Sweeping the potential further in the negative direction to 200 mV (on the left side with respect to the C4 peak) induces new structural changes. The expanded phase is being converted into the compressed one resulting in a smoothing of the surface as shown in Figure 9E,F. This observation makes us think that the C4 peak in the CV is a result of a transition from the expanded into the compressed $(\sqrt{3} \times \sqrt{3})R30°$ structure of the silver adlayer. Interestingly, stepping back the potential to 400 mV induces the reverse transition from compressed to expanded structures. Such experimental evidence shows for the first time that the process of Ag UPD on Au(111) in $[BMI]^+[AlCl_4]^-$ undergoes a completely different scenario in comparison with that in aqueous solutions.

As seen in Figure 10 with respect to the second UPD of Ag, we have found that in terms of STM approaching the potentials in the range 120−100 mV nearly all the monatomically deep holes in the silver adlayer are filled, giving approximate coverage of 1 ML as determined from coulometry (Figure 4). Further reducing the potential to 50 mV causes a rapid formation of a second and third layer of Ag, approaching the overpotential deposition region.

IV. Summary

In this paper, we have studied and compared in detail underpotential deposition of Ag on Au(111) in two distinct solutions: aqueous and ionic electrolytes. Also, we have shown how strongly the differences in the solvent−adatom interactions influence the UPD processes of silver.

(a) In aqueous solutions, the first UPD process of Ag occurs at 520 mV resulting in an expanded homogeneous (3×3) adlayer of Ag, whereas the second one at 25 mV shows a transition from a more open (3×3) structure to a close-packed (1×1) monolayer.

(b) In ionic electrolyte, the first UPD process of Ag exhibits two CV peaks at 410 mV and 230 mV and is characterized by a charge density of 130 μC cm^{-2}. Atomically resolved STM images in this potential range show for the first time a structural transition from an inhomogeneous to an ordered phase with a $(\sqrt{3} \times \sqrt{3})R30°$ structure and adsorbed $AlCL_4^-$ anions with a superlattice of $(1.65 \times \sqrt{3})R30°$ preceding the UPD of Ag. Since we do not know how $AlCl_4^-$ anions bind with the substrate and the adlayer of Ag, it is difficult to conclude whether the inhomogeneous adlayer of Ag is a result of specific adsorption reflecting the different adatom−solvent interactions. The second UPD process of Ag arises at 120 mV and 106 mV, yielding 1 ML of Ag.

(c) In both electrolytes, formation of 1 ML of Ag was found in the UPD range. The dissolution of the Ag adlayer leads to monatomically deep characteristic holes or pits in the gold substrate, which is a signature of 2D surface alloying. In contrast to aqueous solutions where a homogeneous (3×3) adlayer is formed, in ionic electrolyte the inhomogeneous adlayer resembles wormlike connective structures which are indicative of surface alloying governed by spinodal decomposition.

Acknowledgment. This work has been kindly supported by the DFG Center of the Functional Nanostructures (CFN). One of us (C.L.A.) would like to thank the Humboldt Foundation for the fellowship granted.

References and Notes

(1) Kolb, D. M. *Frontiers in Surface and Interface Science*; Duke, C. G., Plummer, E. W., Eds.; Elsevier: Amsterdam, 2002.
(2) Itaya, K. *Prog. Surf. Sci.* **1998**, *58*, 121.
(3) Budevski, E.; Staikov, G.; Lorenz, W. J. *Electrochemical Phase Formation and Growth*; VCH: Weinheim, 1996.
(4) Lorenz, W. J.; Staikov, G.; Schindler, W.; Wiesbeck, W. *J. Electrochem. Soc.* **2002**, *149*, K47−K59.
(5) Wandlowski, Th. In *Thermodinamics and Electrified Interfaces*; Bard, A. J., Stratmann, M., Eds.; Wiley-VCH: Weinheim, 2002; Vol. 1.
(6) Broeckmann, P. In *Solid−Liquid Interfaces*; Wandelt, K., Thurgate, Eds.; Springer: Berlin, 2003.
(7) Zell, C. A.; Endres, F.; Freyland, W. *Phys. Chem. Chem. Phys.* **1999**, *1*, 697−704.
(8) Zell, C. A.; Freyland, W. *Langmuir* **2003**, *19*, 7445−7450.
(9) Freyland, W.; Zell, C. A.; El-Abedin, S. Z.; Endres, F. *Electrochim. Acta* **2003**, *48*, 3053−3061.
(10) Mukhopadhyay, I.; Freyland, W. *Chem. Phys. Lett.* **2003**, *377*, 223−228.
(11) Staub, R.; Alliata, D. *Rev. Sci. Instrum.* **1995**, *66*, 2513−2516.
(12) Itaya, K. *Nanotechnology* **1992**, *3*, 185−187.
(13) Esplandiu, M. J.; Schneeweiss, M. A.; Kolb, D. M. *Phys. Chem. Chem. Phys.* **1999**, *1*, 4847−4854.
(14) Mrozek, P.; Sung, Y.-E.; Wieckowski, A. *Surf. Sci.* **1995,** *335*, 44−51.
(15) Chen, C. H.; Vesecky, S. M.; Gewirth, A. A. *J. Am. Chem. Soc.* **1992**, *114*, 451−458.
(16) Magnussen, O. M.; Hageboeck, J.; Hotlos, J.; Behm, R. J. *Faraday Discuss.* **1992**, *94* 329−338.
(17) Edens, G. J.; Gao, X.; Weaver, M. J. *J. Electroanal. Chem.* **1994**, *375*, 357−366.
(18) Mrozek, P.; Sung, Y.-E.; Han, M.; Gamboa-Aldeco, M.; Wieckowski, A.; Chen, C.-H.; Gewirth, A. A. *Electrochim. Acta* **1995**, *40*, 17−28.
(19) Roughly 400 mV vs Ag/Ag$^+$ corresponds to 0 mV vs SCE.
(20) Schneeweiss, M. A.; Kolb, D. M. *Solid State Ionics* **1997**, *94*, 171−179.
(21) Trevor, D. J.; Chidsey, Ch. E. D.; Loiacono, D. N. *Phys. Rev. Lett.* **1989**, *62*, 929−932.
(22) Stafford, G. R.; Jovic, V. D.; Moffat, T. P.; Zhu, Q.; Jones, S.; Hussey, C. L. *Proc. Electrochem. Soc.* **2000**, *99−41* (Molten Salts XII).
(23) Ye, Shen; Ishibashi, C.; Uosaki, K. *Langmuir* **1999**, *15*, 807−812.
(24) John, D.; Porter, T. R. *J. Phys. Chem.* **1993**, *97*, 6696−6709.
(25) Dogel, J.; Tsekov, R.; Freyland, W. *J. Chem. Phys.* In press.